Reconsideration of the inclusive prompt photon production at LHC with k_T-factorization

A.V. Lipatov[1,2], M.A. Malyshev[1]

August 3, 2016

[1] *Skobeltsyn Institute of Nuclear Physics, Lomonosov Moscow State University, 119991 Moscow, Russia*
[2] *Joint Institute for Nuclear Research, Dubna 141980, Moscow region, Russia*

Abstract

We reconsider the inclusive production of isolated prompt photons in pp collisions at the LHC energies in the framework of k_T-factorization approach. Our analysis is based on the $\mathcal{O}(\alpha\alpha_s)$ off-shell (depending on the transverse momenta of initial quarks and gluons) production amplitudes of $q^*g^* \to \gamma q$ and $q^*\bar{q}^* \to \gamma g$ partonic subprocesses and transverse momentum dependent (or unintegrated) quark and gluon densities in a proton, which are chosen in accordance with the Kimber-Martin-Ryskin prescription. We show that the sub-leading high-order $\mathcal{O}(\alpha\alpha_s^2)$ contributions, not covered by the non-collinear evolution of parton densities, are important to describe latest LHC data.

PACS number(s): 12.38.-t, 13.85.-t

Prompt photon production at hadron colliders is presently of considerable interest from both theoretical and experimental points of view [1–3]. It provides a direct probe of the hard subprocess dynamics because the produced photons are largely insensitive to the effects of final-state hadronization. The measured cross sections are sensitive to the parton (quark and gluon) content of a proton since, at the leading order (LO), the prompt photons are produced mainly via quark-gluon Compton scattering or quark-antiquark annihilation. Prompt photon production represents an important background to many processes involving photons in the final state, including Higgs boson production [4]. Therefore, it is essential to have accurate QCD predictions for corresponding cross sections.

The CMS and ATLAS Collaborations have reported measurements [1, 2] of the inclusive prompt photon production at the LHC energy $\sqrt{s} = 7$ TeV. First measurements of inclusive photon cross sections at $\sqrt{s} = 8$ TeV have been presented by the ATLAS Collaboration very recently [3]. These measurements extend the previous ones to wider ranges of photon pseudorapidity η^γ and transverse energy E_T^γ, up to $E_T^\gamma \sim 1.5$ TeV. The pQCD predictions [5, 6] calculated at the next-to-leading order (NLO) agree with the LHC data within the theoretical and experimental uncertainties, although tend to underestimate the ATLAS data [2] at $E_T^\gamma \sim 100$ GeV and overestimate the CMS data [1] at lower $E_T^\gamma \sim 40$ GeV. An alternative QCD description can be achieved in the framework of k_T-factorization approach [7, 8], which is based on the small-x Balitsky-Fadin-Kuraev-Lipatov (BFKL) [9] evolution equation and provides solid theoretical grounds for the effects of initial gluon radiation and intrinsic parton transverse momentum. The latter is known to be important for description of the prompt photon production at hadron colliders [10, 11], and the high-energy resummation formalism was applied for photon production [12, 13].

In the present note we give a systematic analysis of recent LHC data [1–3] using the k_T-factorization approach. Our consideration below is mainly based on the $\mathcal{O}(\alpha\alpha_s)$ off-shell (depending on the transverse momenta of initial quarks and gluons) quark-gluon Compton scatterring or quark-antiquark annihilation subprocesses. We see certain advantages in the fact that, even with the LO partonic amplitudes, one can include a large piece of high-order corrections (namely, part of NLO + NNLO terms and terms containing leading $\log 1/x$ enhancement of cross sections due to real parton emissions in initial state, according to the BFKL evolution) taking them into account in the form of transverse momentum dependent (TMD) parton densities[1]. It is known that such terms give the main contribution to the production cross section at high energies. Unlike earlier calculations [15–19], to evaluate the off-shell production amplitudes we employ the reggeized parton approach [20–22] based on the effective action formalism [23], that ensures the gauge invariance of obtained amplitudes despite the off-shell initial quarks and gluons[2] and therefore significantly improves previous considerations [15–19]. We choose the TMD parton densities in a proton in accordance with the Kimber-Martin-Ryskin (KMR) prescription [24], currently explored at the NLO [25], and examine an assumption [18] on the TMD sea quark densities in a proton applied in our previous consideration [19]. The numerical effect of this approximation is specially investigated below. In addition, we take into account some $\mathcal{O}(\alpha\alpha_s^2)$ contributions, namely $qq' \to \gamma qq'$ ones. The latter probe essential large x (see below) and therefore can be calculated in the traditional collinear QCD factorization scheme. Thus, we rely on a combination of

[1] A detailed description of the k_T-factorization approach can be found, for example, in reviews [14].

[2] The investigation [19] was based on the off-shell partonic amplitudes gauge-invariant in a small-x limit.

two techniques with each of them being used where it is most suitable. The improvement of our previous predictions [19] as it described above is a special goal of present note.

Let us start from a short review of calculation steps. We describe first the evaluation of the off-shell amplitudes of quark-gluon Compton scattering and quark-antiquark annihilation subprocesses:

$$q^*(k_1) + g^*(k_2) \to \gamma(p_1) + q(p_2), \tag{1}$$

$$q^*(k_1) + \bar{q}^*(k_2) \to \gamma(p_1) + g(p_2), \tag{2}$$

where the four-momenta of corresponding particles are given in the parentheses. In the center-of-mass frame of colliding protons, having four-momenta l_1 and l_2, we define

$$k_1 = x_1 l_1 + k_{1T}, \quad k_2 = x_2 l_2 + k_{2T}, \tag{3}$$

where x_1 and x_2 are the longitudinal momentum fractions of the protons carried by the interacting off-shell partons having transverse four-momenta k_{1T} and k_{2T} (note that $k_{1T}^2 = -\mathbf{k}_{1T}^2 \neq 0$, $k_{2T}^2 = -\mathbf{k}_{2T}^2 \neq 0$). In the reggeized parton approach the off-shell amplitude of subprocess (1) reads:

$$\mathcal{A}(q^*g^* \to \gamma q) = ee_q\, g\, t^a \epsilon^\mu(p_1)\epsilon^\nu(k_2)\, \bar{v}_{s_1}(p_2)\, \mathcal{A}^{\mu\nu}(q^*g^* \to \gamma q)\, u_{s_2}(x_1 l_1), \tag{4}$$

where e and e_q are the electron and quark (fractional) electric charges, g is the strong charge, a is the eight-fold color index, $\epsilon^\mu(p_1)$ and $\epsilon^\nu(k_2)$ are the polarization four-vectors and

$$\mathcal{A}^{\mu\nu}(q^*g^* \to \gamma q) = \gamma^\nu \frac{\hat{k}_1 - \hat{p}_1}{(k_1 - p_1)^2}\Gamma^\mu_{(+)}(k_1, p_1) + \gamma^\mu \frac{\hat{k}_1 + \hat{k}_2}{(k_1 + k_2)^2}\Gamma^\nu_{(+)}(k_1, -k_2) + \\ + \hat{k}_1 \frac{l_1^\mu l_1^\nu}{(l_1 \cdot k_2)(l_1 \cdot p_1)}. \tag{5}$$

The latter term in (5) is the induced term, and we neglected the quark masses. The off-shell amplitude of subprocess (2) reads:

$$\mathcal{A}(q^*\bar{q}^* \to \gamma g) = ee_q\, g\, t^a \epsilon^\mu(p_1)\epsilon^\nu(p_2)\, \bar{v}_{s_1}(x_2 l_2)\, \mathcal{A}^{\mu\nu}(q^*\bar{q}^* \to \gamma g)\, u_{s_2}(x_1 l_1), \tag{6}$$

where

$$\mathcal{A}^{\mu\nu}(q^*\bar{q}^* \to \gamma g) = \Gamma^\nu_{(-)}(k_2, p_2)\frac{\hat{k}_1 - \hat{p}_1}{(k_1 - p_1)^2}\Gamma^\mu_{(+)}(k_1, p_1) + \Gamma^\mu_{(-)}\frac{\hat{k}_1 - \hat{p}_2}{(k_1 - p_2)^2}\Gamma^\nu_{(+)}(k_1, k_2) + \\ + \hat{k}_1 \frac{l_1^\mu l_1^\nu}{(l_1 \cdot k_2)(l_1 \cdot p_1)} - \hat{k}_2 \frac{l_2^\mu l_2^\nu}{(l_2 \cdot k_2)(l_2 \cdot p_1)}. \tag{7}$$

The effective vertices read [20, 21]:

$$\Gamma^\mu_{(+)}(k, q) = \gamma^\mu - \hat{k}\frac{l_1^\mu}{(l_1 \cdot q)}, \tag{8}$$

$$\Gamma^\mu_{(-)}(k, q) = \gamma^\mu - \hat{k}\frac{l_2^\mu}{(l_2 \cdot q)}, \tag{9}$$

The summation on the final state photon and gluon polarizations is carried out with the usual covariant formula:

$$\sum \epsilon^{\mu}(p)\epsilon^{*\,\nu}(p) = -g^{\mu\nu}. \tag{10}$$

In contrast, according to the k_T-factorization prescription [7, 8], the summation over the polarizations of incoming off-shell gluons is carried with

$$\sum \epsilon^{\mu}(k)\epsilon^{*\,\nu}(k) = \frac{\mathbf{k}_T^{\mu}\mathbf{k}_T^{\nu}}{\mathbf{k}_T^2}. \tag{11}$$

In the limit of collinear QCD factorization, when $\mathbf{k}_T^2 \to 0$, this expression converges to the ordinary one after averaging on the azimuthal angle. The spin density matrix for all initial off-shell spinors in the parton reggezation approach is taken in the usual form:

$$\sum u(x_i l_i)\bar{u}(x_i l_i) = x_i \hat{l}_i, \tag{12}$$

where $i = 1$ or 2 and we omittd the spinor indices. Further calculations are straightforward and in other respects follow the standard QCD Feynman rules. The evaluation of traces was performed using the algebraic manipulation system FORM [26].

To calculate the contributions of subprocesses (1) and (2) to the prompt photon production cross section we have to convolute the relevant partonic cross sections and the TMD parton densities in a proton:

$$\begin{aligned}\sigma(pp \to \gamma + X) = \sum_{a,b} \int \frac{1}{16\pi (x_1 x_2 s)^2} f_a(x_1, \mathbf{k}_{1T}^2, \mu_F^2) f_b(x_2, \mathbf{k}_{2T}^2, \mu_F^2) \times \\ \times |\bar{\mathcal{A}}(a^* b^* \to \gamma c)|^2 d\mathbf{k}_{1T}^2 d\mathbf{k}_{2T}^2 d\mathbf{p}_{1T}^2 dy_1 dy_2 \frac{d\phi_1}{2\pi}\frac{d\phi_2}{2\pi},\end{aligned} \tag{13}$$

where a, b and c are parton indices (q or g), $f_a(x, \mathbf{k}_T^2, \mu_F^2)$ are the TMD parton densities at the factorization scale μ_F, s is the total energy, y_1 and y_2 are the center-of-mass rapidities of final state particles, and ϕ_1 and ϕ_2 are the azimuthal angles of initial partons.

As it was mentioned above, we take into account additional contribution from $qq' \to \gamma qq'$ subprocess. We apply here the collinear limit of formulas obtained earlier [18, 19].

It is well-known that the photon production cross section suffers from a final state divergence when the photon becomes collinear to the outgoing parton. This collinear divergence cannot be removed by adding the virtual corrections and is usually absorbed into the parton-to-photon fragmentation functions. In the present note we used an approach proposed in [18]. So, the standard QCD perturbation theory can be only applied when the wavelength of the emitted photon (in the emitting quark rest frame) becomes larger than the typical hadronic scale $\mathcal{O}(1\ \mathrm{GeV}^{-1})$. Below this scale, the non-perturbative effects of photon fragmentation take place and have to be taken into account. Accordingly, we split the photon cross section into two pieces:

$$\sigma = \sigma_{\mathrm{pert}}(\mu_{\mathrm{reg}}^2) + \sigma_{\mathrm{non-pert}}(\mu_{\mathrm{reg}}^2), \tag{14}$$

where $\sigma_{\mathrm{pert}}(\mu_{\mathrm{reg}}^2)$ is the perturbative contribution and $\sigma_{\mathrm{non-pert}}(\mu_{\mathrm{reg}}^2)$ is the non-perturbative one which includes the fragmentation component. Both of them depend on the regularization scale μ_{reg}, which can be used to separate these two pieces. Following [18], we restrict $\sigma_{\mathrm{pert}}(\mu_{\mathrm{reg}}^2)$ to the region $M \geq \mu_{\mathrm{reg}}$, where M is the invariant mass of the photon + parton

subsystem and $\mu_{\rm reg} \sim 1$ GeV is the typical hadronic scale. Under this condition, the contribution $\sigma_{\rm pert}(\mu^2_{\rm reg})$ is free from collinear divergences. The sensitivity of our results to the choice of $\mu_{\rm reg}$ is reasonably soft[3] and investigated below.

Next, the size of conventional fragmentation contribution is dramatically reduced by the photon isolation criterion introduced in the experimental analyses [1–3], mainly to reduce huge background. This criterion is the following: a photon is isolated if the amount of hadronic transverse energy $E_T^{\rm had}$ deposited inside a cone with aperture R centered around the photon direction in the pseudo-rapidity and azimuthal angle plane, is smaller than some value $E_T^{\rm max}$:

$$\begin{gathered} E_T^{\rm had} \leq E_T^{\rm max}, \\ (\eta^{\rm had} - \eta^\gamma)^2 + (\phi^{\rm had} - \phi^\gamma)^2 \leq R^2. \end{gathered} \tag{15}$$

The CMS Collaboration takes $R = 0.4$ and $E_T^{\rm max} = 5$ GeV [1], whereas the ATLAS Collaboration applies $E_T^{\rm max} = 7$ GeV [2] or $E_T^{\rm max} = 4.8$ GeV $+ 4.2 \cdot 10^{-3} \times E_T^\gamma$ [3] with the same R. According to the estimates [1–3], after applying the isolation cut the fragmentation contribution amounts to about 10% of the measured cross section. This value is smaller than the typical theoretical uncertainties in calculating the perturbative contribution $\sigma_{\rm pert}(\mu^2_{\rm reg})$. Moreover, the isolation criterion (15), applied in our calculations, is used as a tool to remove the non-perturbative part of cross section (14), where final photon is radiated close to quark (inside the isolation cone).

To calculate the TMD parton densities in a proton we adopt the KMR prescription [24] developed at the NLO [25]. The KMR approach is a formalism to construct the TMD parton densities from the known conventional parton distributions. The key assumption is that the k_T dependence enters at the last evolution step, so that the Dokshitzer-Gribov-Lipatov-Altarelli-Parisi (DGLAP) evolution [27] can be used up to this step. Numerically, for the input we applied parton densities from the MSTW'2008 NLO set [28].

Other essential parameters we take as follows: renormalization and factorization scales $\mu_R = \mu_F = \xi E_T^\gamma$, where the unphysical parameter ξ is varied between 1/2 and 2 about the default value $\xi = 1$ to estimate the scale uncertainties of our calculations. The uncertainties originating from the cut-off parameter M are estimated in the same way, by varying M between $0.5 < M < 2$ GeV about the default value $M = 1$ GeV. We apply the two-loop formula for the strong coupling constant with $n_f = 5$ active quark flavours at $\Lambda_{\rm QCD} = 226.2$ MeV and use the running QED coupling constant over a wide region of E_T^γ, as it is measured by the ATLAS Collaboration. The same renormalization scale μ_R is applied for both the QCD and QED coupling constants. Everywhere the multidimensional integration have been performed by the means of Monte Carlo technique, using the routine VEGAS [29].

We now are in a position to present our numerical results in comparison with the LHC data [1–3]. So, the CMS Collaboration has measured the prompt photon production cross section as a function of the photon transverse energy E_T^γ in the kinematical region defined by $25 < E_T^\gamma < 400$ GeV and $|\eta^\gamma| < 2.5$ at $\sqrt{s} = 7$ TeV [1]. The ATLAS Collaboration has measured the photon cross sections as a functions of transverse energy and pseudorapidity in the kinematic range $100 < E_T^\gamma < 1000$ GeV, $|\eta^\gamma| < 1.37$ and $1.52 < |\eta^\gamma| < 2.37$ at $\sqrt{s} = 7$ TeV [2]. Recently, the data taken at $\sqrt{s} = 8$ TeV in the kinematic range $25 < E_T^\gamma < 1500$ GeV, $|\eta^\gamma| < 0.6$, $0.6 < |\eta^\gamma| < 1.37$, $1.56 < |\eta^\gamma| < 1.81$ and $1.81 < |\eta^\gamma| < 2.37$ were

[3]Under the isolation condition, see below.

presented by the ATLAS Collaboration [3]. The results of our calculations are shown in Figs. 1 — 7. In Figs. 1, 2 and 4 we confront the cross sections calculated as a function of E_T^γ with the LHC data and plot corresponding data/theory ratios. As one can see from Fig. 2, our results agree well with the ATLAS data taken at $\sqrt{s} = 7$ TeV and central pseudorapidities $|\eta^\gamma| < 1.37$ in the whole E_T^γ region within the experimental and theoretical uncertainties. At $\sqrt{s} = 8$ TeV, perfect agreement with the recent ATLAS data for all E_T^γ is achieved at $|\eta^\gamma| < 0.6$, see Fig. 4. In the next pseudorapidity subdivision, $0.6 < |\eta^\gamma| < 1.37$, the overall description of the data is rather satisfactory, although a some tendence to slightly underestimate the data at high $E_T^\gamma > 200$ GeV can be seen. In the forward region, where $1.52 < |\eta^\gamma| < 2.37$, our predictions lie somewhat below the ATLAS data, for both $\sqrt{s} = 7$ and 8 TeV. This becomes clearer in the η^γ distributions, presented by the ATLAS Collaboration for the first time (see Fig. 3). The observed discrepancy could be attributed to the missing higher-order contributions, not taken into account in our consideration. However, we note that the ATLAS data in these subdivisions of η^γ are close to the upper bound of theoretical uncertainties. The CMS data are more or less well described for all pseudorapidities η^γ (see Fig. 1), although our predictions tend to slightly overestimate the data at low E_T^γ and underestimate them at high E_T^γ, that could be due to the TMD parton densities, involved in the calculations. In the forward kinematical region, where $2.1 < \eta^\gamma < 2.5$, the CMS data are described better compared to the ATLAS ones.

Let us turn to comparison of obtained results with the predictions based on a special assumption [18] on the TMD sea quark density in a proton, which was used in our previous consideration [19]. The proposed scheme is based on the separation of the TMD sea quark densities to the sea quarks appearing at the last step of the gluon evolution and ones coming from the earlier (second-to-last, third-to-last and other) gluon splittings. First of them are calculated using $\mathcal{O}(\alpha\alpha_s^2)$ off-shell gluon-gluon fusion subprocess, $g^*g^* \to \gamma q\bar{q}$. To estimate the second contributions the specific properties of the KMR formalism, which enables us to discriminate between the various components of the TMD quark densities (see [18, 19]), are used. The predictions based on this scheme are shown in Figs. 1 — 4 by the dashed curves. We find that these predictions reproduce well the recent LHC data [1–3] at the central rapidities (that agrees with the conclusions given in [19]) and underestimate them in a forward region. They lie somewhat below the newly presented calculations, although both of them are rather close to each other and, in general, coincide within the theoretical uncertainties. Nevertheless, the latter describe better the latest ATLAS data [2, 3].

The relative contributions to prompt photon production cross sections are shown in Figs. 5 — 7. As it was expected, the off-shell quark-gluon Compton scattering subprocess dominates at low and moderate photon transverse energies. The $\mathcal{O}(\alpha\alpha_s^2)$ contributions from $qq' \to \gamma qq'$ subprocess play a role mainly at high E_T^γ, where the large-x region is probed. It supports our assumptions that these subprocesses can be safely taken into account in the framework of collinear QCD factorization, thus avoiding an unnecessary complications of consideration. However, these terms are important to describe the data. The contribution of off-shell quark-antiquark annihilation is negligible at the LHC conditions.

To conclude, we presented here analysis of latest LHC data on the inclusive prompt photon production at $\sqrt{s} = 7$ and 8 TeV in the framework of k_T-factorization approach. Unlike previous studies, our consideration was based on the $\mathcal{O}(\alpha\alpha_s)$ off-shell partonic amplitudes calculated in the reggeized parton approach, that ensures their exact gauge invariance even

with the off-shell initial partons. In this way, even with the LO hard scaterring amplitudes, we include a large piece of high-order QCD corrections taking them into account in the form of TMD parton densities. To be precise, in the framework of KMR prescription used, we include the NLO terms containing $\log 1/x$ enhancement of the cross section connected with the initial-state real parton emissions. Such terms are known as giving the main high-order corrections to the cross section at high energies[4]. Of course, other high-order contributions, like virtual radiative corrections, are not taken into account in our approach. We achieved reasonably good agreement between our predictions and the CMS data for $E_T^\gamma \leq 100$ GeV in the whole region of photon pseudorapidity, $|\eta^\gamma| < 2.5$. At higher E_T^γ, our predictions tend to underestimate the CMS data. The ATLAS data are described well in the central pseudorapidity region, where $|\eta^\gamma| < 1.37$. We showed that the sub-leading higher-order $\mathcal{O}(\alpha\alpha_s^2)$ contributions, not covered by the non-collinear parton evolution, are important to describe the LHC data, especially at high E_T^γ. We examined the numerical effect of the special assumption [18] on the TMD sea quark densities in a proton used in the previous consideration [19], and found that our newly presented results describe a little better the latest ATLAS data [2,3].

Acknowledgements. The authors are very grateful to S. Baranov and H. Jung for very useful discussions and important remarks. This work was supported in part by RFBR grant 16-32-00176-mol-a, grant of the President of Russian Federation NS-7989.2016.2 and by the DESY Directorate in the framework of Moscow-DESY project on Monte-Carlo implementations for HERA-LHC.

References

[1] CMS Collaboration, Phys. Rev. D **84**, 052011 (2011).

[2] ATLAS Collaboration, Phys. Rev. D **89**, 052004 (2014).

[3] ATLAS Collaboration, arXiv:1605.03495 [hep-ex].

[4] CMS Collaboration, J. Phys. G **34**, 995 (2007).

[5] S. Catani, M. Fontannaz, J.-P. Guillet, E. Pilon, JHEP **05**, 028 (2002).

[6] P. Aurenche, M. Fontannaz, J.-P. Guillet, Phys. Rev. D **73**, 094007 (2006).

[7] L.V. Gribov, E.M. Levin, M.G. Ryskin, Phys. Rep. **100**, 1 (1983);
E.M. Levin, M.G. Ryskin, Yu.M. Shabelsky, A.G. Shuvaev, Sov. J. Nucl. Phys. **53**, 657 (1991).

[8] S. Catani, M. Ciafaloni, F. Hautmann, Nucl. Phys. B **366**, 135 (1991);
J.C. Collins, R.K. Ellis, Nucl. Phys. B **360**, 3 (1991).

[4]The part of collinear NNLO pQCD corrections, namely, $\log 1/x$-enhanced terms, are effectively taken into account in the calculations based on the scheme [18,19].

[9] E.A. Kuraev, L.N. Lipatov, V.S. Fadin, Sov. Phys. JETP **44**, 443 (1976);
E.A. Kuraev, L.N. Lipatov, V.S. Fadin, Sov. Phys. JETP **45**, 199 (1977);
I.I. Balitsky, L.N. Lipatov, Sov. J. Nucl. Phys. **28**, 822 (1978).

[10] S. Catani, M.L. Mangano, P. Nason, C. Oleari, W. Vogelsang, JHEP **9903**, 025 (1999).

[11] N. Kidonakis, J.F. Owens, Phys. Rev. D **61**, 094004 (2000).

[12] G. Diana, Nucl. Phys. B **824**, 154 (2010).

[13] G. Diana, J. Rojo, R. Ball, Phys. Lett. B **693**, 430 (2010).

[14] B. Andersson *et al.* (Small-x Collaboration), Eur. Phys. J. C **25**, 77 (2002);
J. Andersen *et al.* (Small-x Collaboration), Eur. Phys. J. C **35**, 67 (2004);
J. Andersen *et al.* (Small-x Collaboration), Eur. Phys. J. C **48**, 53 (2006).

[15] M.A. Kimber, A.D. Martin, M.G. Ryskin, Eur. Phys. J. C **12**, 655 (2000).

[16] T. Pietrycki, A. Szczurek, Phys. Rev. D **75**, 014023 (2007).

[17] T. Pietrycki, A. Szczurek, Phys. Rev. D **76**, 034003 (2007).

[18] S.P. Baranov, A.V. Lipatov, N.P. Zotov, Phys. Rev. D **77**, 074024 (2008).

[19] A.V. Lipatov, M.A. Malyshev, N.P. Zotov, Phys. Lett. B **699**, 93 (2011).

[20] L.N. Lipatov, M.I. Vyazovsky, Nucl. Phys. B **597**, 399 (2001).

[21] A.V. Bogdan, V.S. Fadin, Nucl. Phys. B **740**, 36 (2006).

[22] M. Hentschinski, A. Sabio Vera, Phys. Rev. D **85**, 056006 (2012);
M. Hentschinski, Nucl. Phys. B **859**, 129 (2012);
G. Chachamis, M. Hentschinski, J.D. Madrigal Martinez, A. Sabio Vera, Nucl. Phys. B **861**, 133 (2012).

[23] L.N. Lipatov, Nucl. Phys. B **452**, 369 (1995); Phys. Rept. **286**, 131 (1997).

[24] M.A. Kimber, A.D. Martin, M.G. Ryskin, Phys. Rev. D **63**, 114027 (2001);
G. Watt, A.D. Martin, M.G. Ryskin, Eur. Phys. J. C **31**, 73 (2003).

[25] A.D. Martin, M.G. Ryskin, G. Watt, Eur. Phys. J. C **66**, 163 (2010).

[26] J.A.M. Vermaseren, NIKHEF-00-023 (2000).

[27] V.N. Gribov and L.N. Lipatov, Sov.J. Nucl. Phys. **15**, 438 (1972);
L.N. Lipatov, Sov. J. Nucl. Phys. **20**, 94 (1975);
G. Altarelli, G. Parisi, Nucl. Phys. B **126**, 298 (1977);
Yu.L. Dokshitzer, Sov. Phys. JETP **46**, 641 (1977).

[28] A.D. Martin, W.J. Stirling, R.S. Thorne, G. Watt, Eur. Phys. J. C **63**, 189 (2009).

[29] G.P. Lepage, J. Comput. Phys. **27**, 192 (1978).

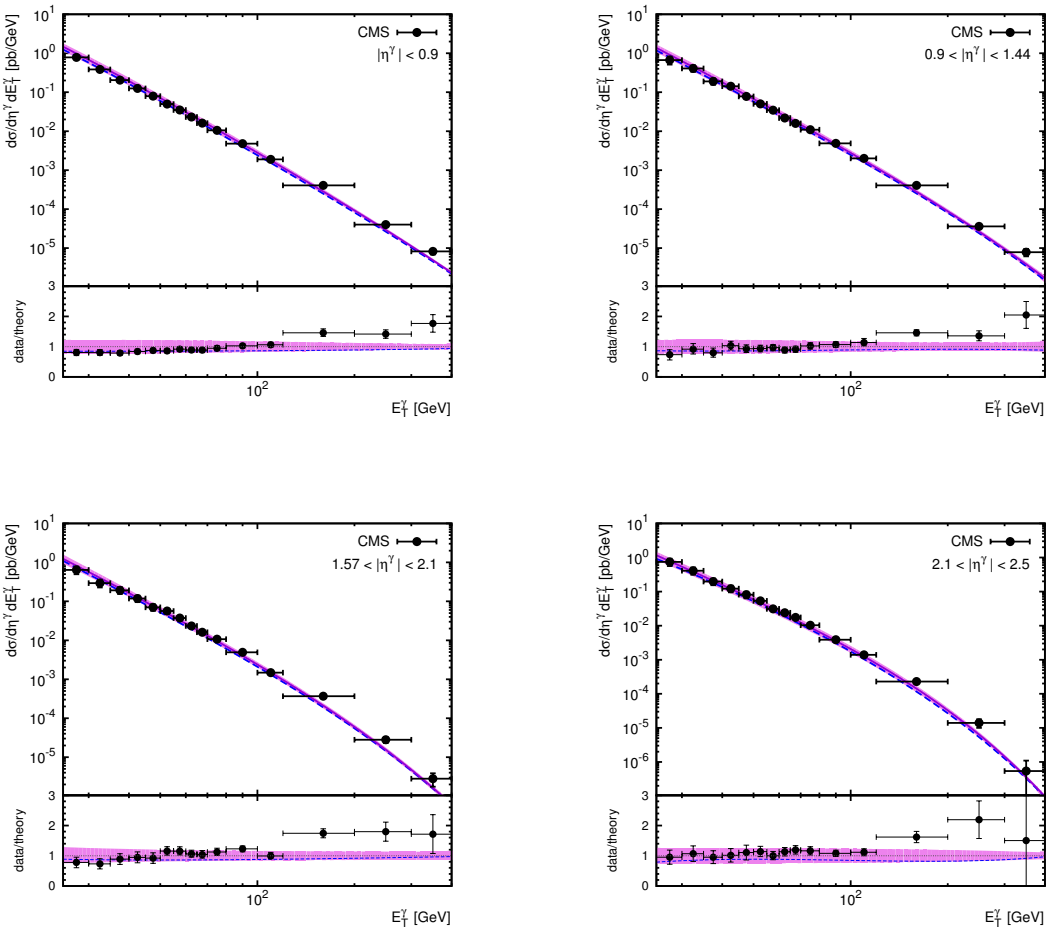

Figure 1: The inclusive prompt photon production at the LHC calculated as a function of photon transverse energy E_T^γ at $\sqrt{s} = 7$ TeV. The solid curves correspond to the predictions obtained with the KMR parton densities at the default scale. The shaded band corresponds to the variation in scales μ_R, μ_F and in parameter $\mu_{\rm reg}$, as described in the text. The dashed curves correspond to the special assumption [18] on the TMD sea quark density, applied as it was done in [19]. The experimental data are from CMS [1].

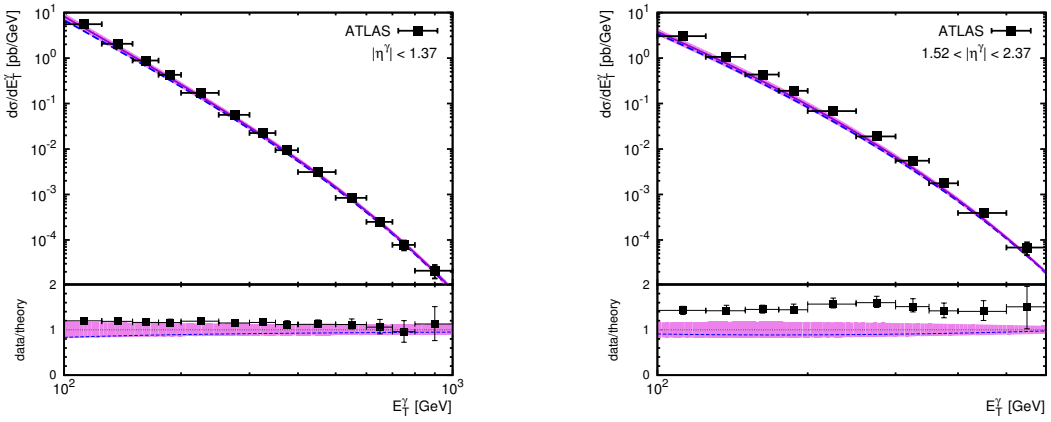

Figure 2: The inclusive prompt photon production at the LHC calculated as a function of photon transverse energy E_T^γ at $\sqrt{s} = 7$ TeV. Notation of all curves is the same as in Fig. 1. The experimental data are from ATLAS [2].

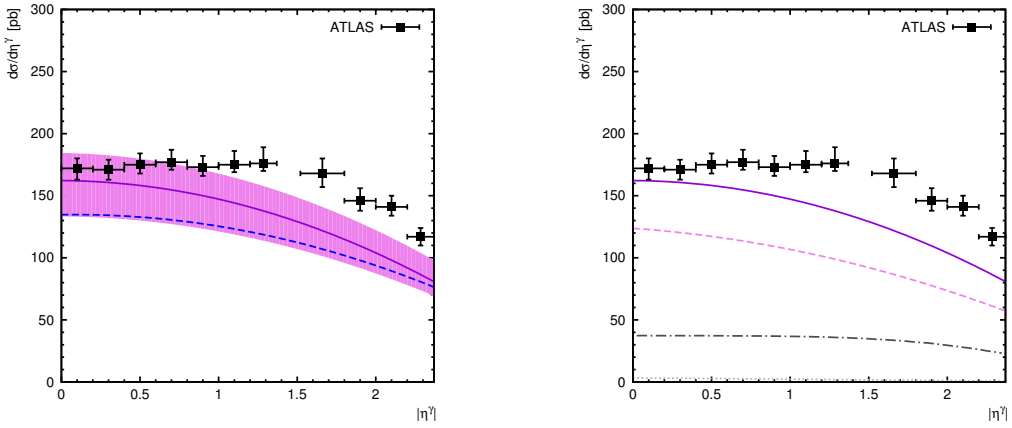

Figure 3: The inclusive prompt photon production at the LHC calculated as a function of photon pseudorapidity η^γ at $\sqrt{s} = 7$ TeV. Different contributions are shown on the right panel. Notation of all curves in the left panel is the same as in Fig. 1. The dashed, dotted and dash-dotted curves in the right panel correspond to the $q^*g^* \to \gamma q$, $q^*\bar{q}^* \to \gamma g$ and $qq' \to \gamma qq'$ subprocesses, while the solid curves represent the sum of all contributions. The experimental data are from ATLAS [2].

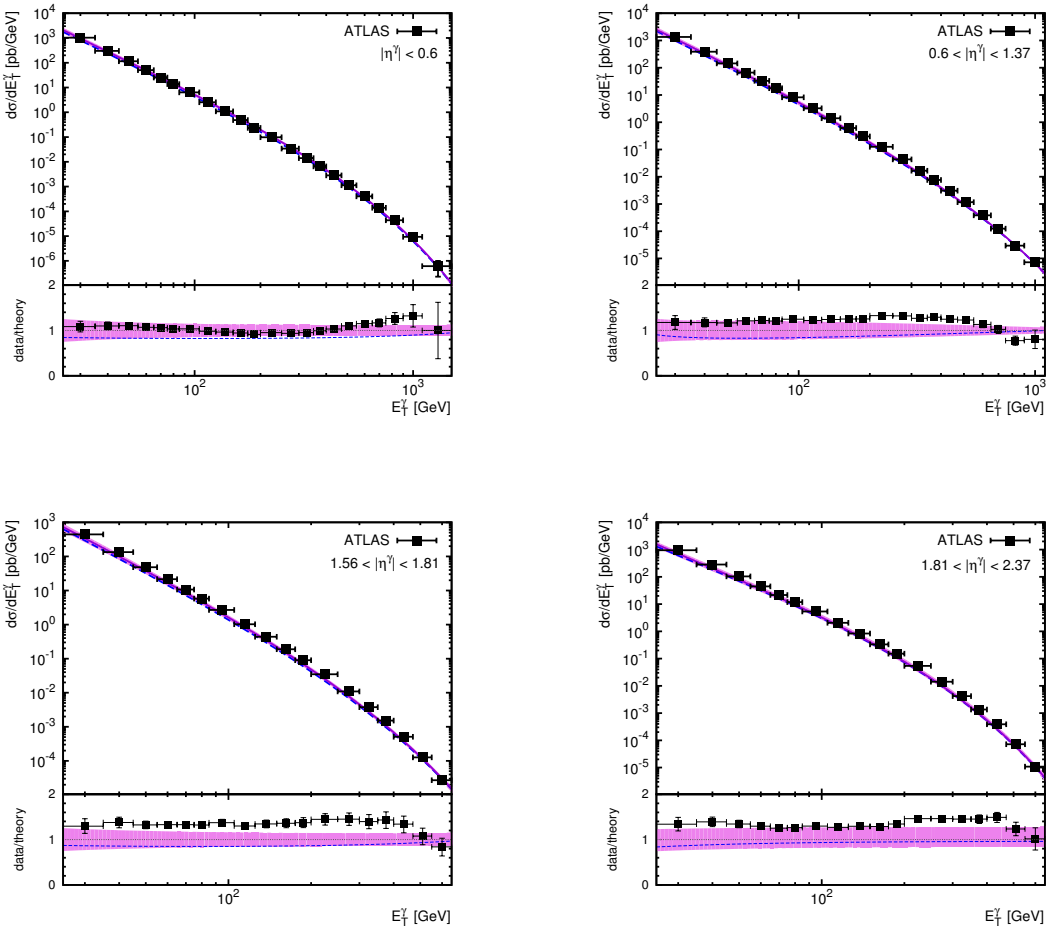

Figure 4: The inclusive prompt photon production at the LHC calculated as a function of photon transverse energy E_T^γ at $\sqrt{s} = 8$ TeV. Notation of all curves is the same as in Fig. 1. The experimental data are from ATLAS [3].

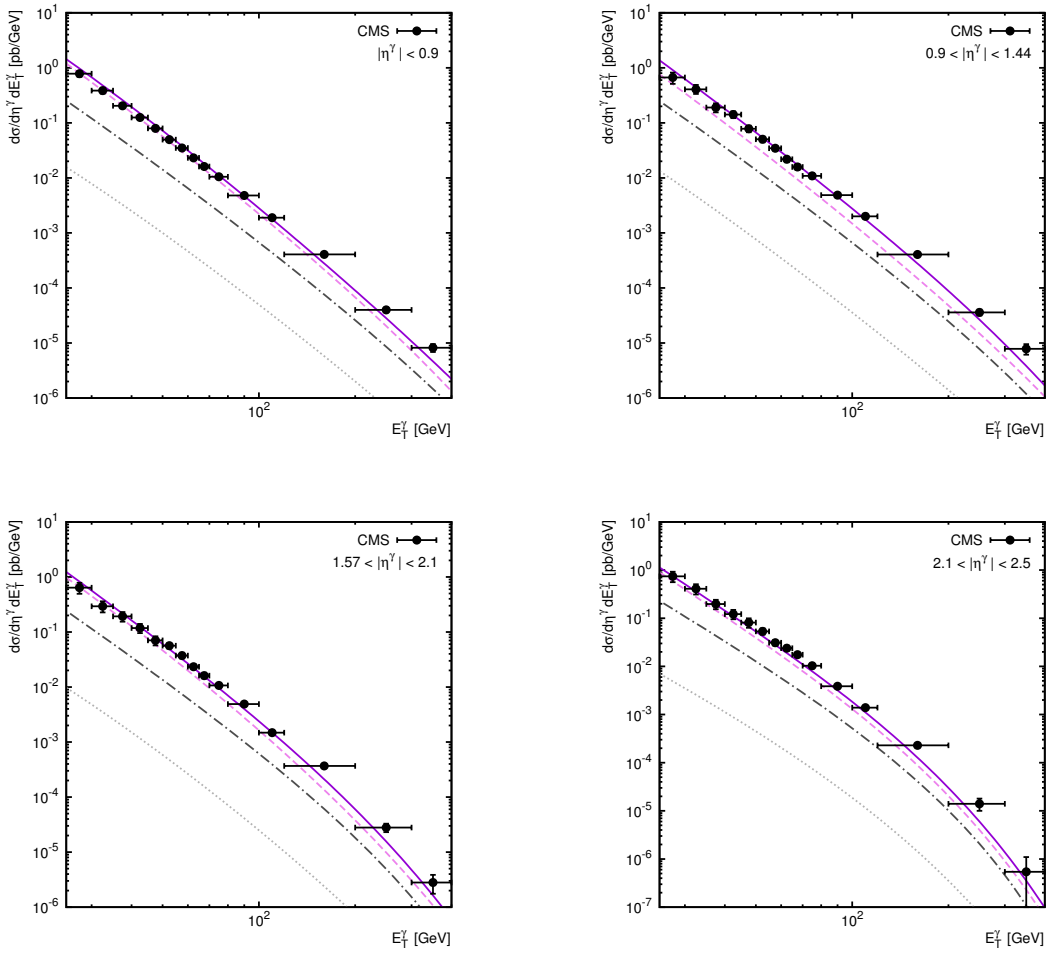

Figure 5: Different contributions to the inclusive prompt photon production cross sections at $\sqrt{s} = 7$ TeV. The dashed, dotted and dash-dotted curves correspond to the $q^*g^* \to \gamma q$, $q^*\bar{q}^* \to \gamma g$ and $qq' \to \gamma qq'$ subprocesses. The solid curves represent the sum of all contributions. The experimental data are from CMS [1].

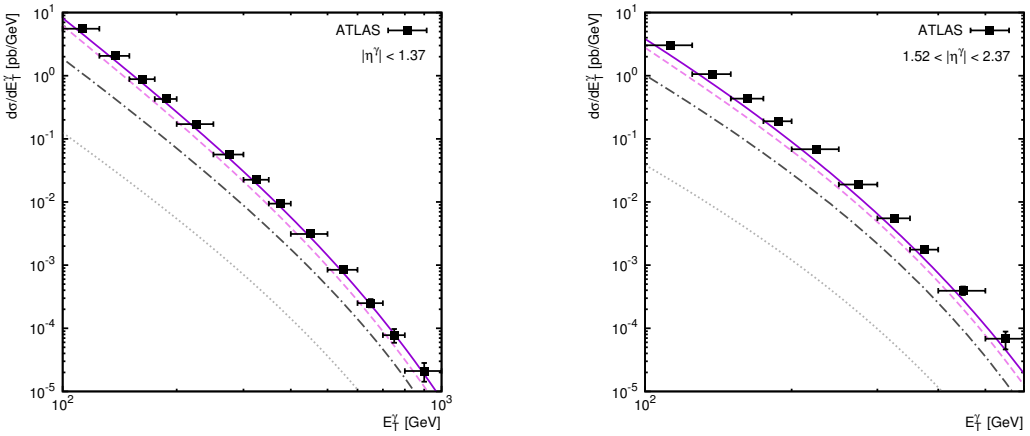

Figure 6: Different contributions to the inclusive prompt photon production cross sections at $\sqrt{s} = 7$ TeV. Notation of all curves is the same as in Fig. 5. The experimental data are from ATLAS [2].

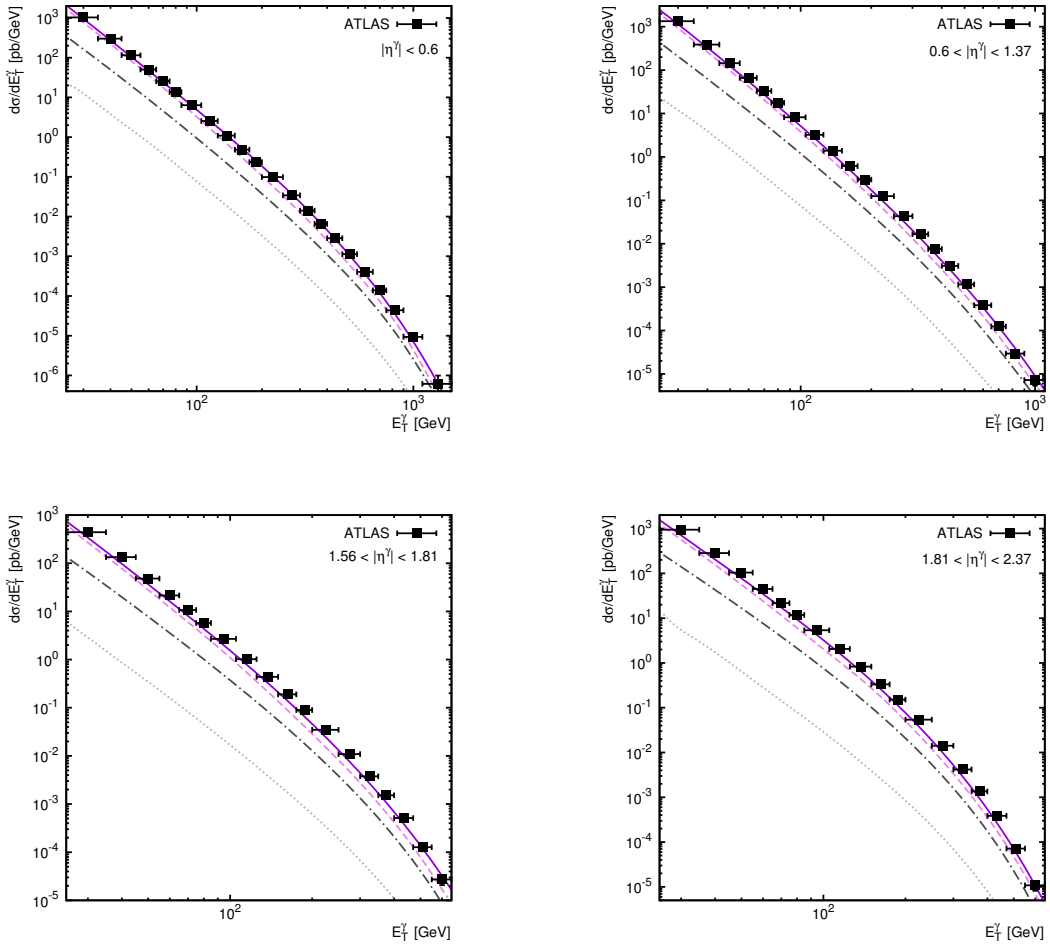

Figure 7: Different contributions to the inclusive prompt photon production cross sections at $\sqrt{s} = 8$ TeV. Notation of all curves is the same as in Fig. 5. The experimental data are from ATLAS [3].